Available online at www.sciencedirect.com
ScienceDirect
Solid State Sciences 10 (2008) 746–753
Solid State Sciences
www.elsevier.com/locate/ssscie

Oxygen-18 surface exchange and diffusion in Li_2O-deficient single crystalline lithium niobate

Peter Fielitz [a,*], Günter Borchardt [a], Roger A. De Souza [b], Manfred Martin [b], Muayad Masoud [c], Paul Heitjans [c]

[a] *Institut für Metallurgie, Technische Universität Clausthal, Robert-Koch-Straße 42, D-38678 Clausthal-Zellerfeld, Germany*
[b] *Institut für Physikalische Chemie, RWTH Aachen, Landoltweg 2, D-52056 Aachen, Germany*
[c] *Institut für Physikalische Chemie und Elektrochemie, and Zentrum für Festkörperchemie und Neue Materialien (ZFM), Leibniz Universität Hannover, Callinstraße 3-3a, D-30167 Hannover, Germany*

Received 14 February 2007; received in revised form 19 July 2007; accepted 18 November 2007
Available online 23 November 2007

Dedicated to Prof. H. Schmalzried on the occasion of his 75th birthday.

Abstract

$^{18}O/^{16}O$ isotope exchange in combination with SIMS depth profiling was used to investigate oxygen transport in Li_2O-deficient single crystalline $LiNbO_3$ in the temperature range $983 \leq T/K \leq 1188$ at 200 mbar oxygen. Within the limit of experimental error and for the investigated range of temperatures no significant differences between transport parallel and transport perpendicular to the *c*-axis were found. The following temperature dependencies were determined: for oxygen tracer diffusion $D = 6.4 \times 10^{-3}\exp[-333\ \text{kJ/mol}/(RT)]\ \text{m}^2/\text{s}$; and for oxygen surface exchange $k = 7.8 \times 10^{2}\exp[-288\ \text{kJ mol}^{-1}/(RT)]$ m/s. The activation enthalpy obtained for tracer diffusion can be interpreted as the enthalpy of migration of extrinsic oxygen vacancies induced by impurities with lower valency on niobium sites.

Keywords: Oxygen diffusion; Oxygen surface exchange; Lithium niobate; Secondary ion mass spectrometry

1. Introduction

Lithium niobate $LiNbO_3$ [below the Curie temperature: space group *R*3*c*; melting point of the congruent composition (48.5 mol% Li_2O): 1526 K; room temperature lattice parameters of the congruent composition: $c = 1.3866$ nm and $a = 0.51502$ nm] is an interesting oxide material especially for both fundamental studies and technological applications. The polar asymmetry of the Li–O ''cage'' gives rise to large ferroelectric, pyroelectric, and piezoelectric coefficients [1–3]. Besides its photorefractive (and photovoltaic) effect [4,5], $LiNbO_3$ possesses useful electro-optic and acousto-optic properties that make it a unique non-linear optical material [3,6,7].

$LiNbO_3$ exists as a non-stoichiometric material with a wide, asymmetric solid solution region, ranging from about 44 mol% Li_2O as the minimum value (at about 1470 K) to about 50.5 mol% Li_2O. The temperature dependence of the solubility on the Li_2O-poor side of the solid solution range is fairly strong while it is virtually zero on the Li_2O-rich side [8]. To explain this non-stoichiometry several defect models have been proposed for $LiNbO_3$ [8–14]. In many applications of $LiNbO_3$ diffusion processes are important for obtaining the required material with tailored properties. Thus, numerous diffusion studies have been performed on single crystalline $LiNbO_3$. The diffusion of impurities such as H, D, Na, Cs, Rb, Ta, Mg, Cu, Co, Zn, Ni, V, Er, Nd, Ca, and Ti was studied by various techniques such as electrical conductivity measurements, nuclear magnetic resonance (NMR), tracer diffusion, thermogravimetry, secondary ion mass spectrometry (SIMS), electron microprobe analysis and Rutherford

* Corresponding author. Tel.: +49 5323 72 2634.
E-mail address: peter.fielitz@tu-clausthal.de (P. Fielitz).

1293-2558/$ - see front matter © 2007 Elsevier Masson SAS. All rights reserved.
doi:10.1016/j.solidstatesciences.2007.11.020

backscattering. A detailed review of all these diffusion studies can be found in Ref. [15]. However, reliable data on the self-diffusion of Li, Nb, and O in $LiNbO_3$ are scarce, and there is no information available on the self-diffusivities of the three constituents in the same well characterised and carefully equilibrated samples.

Lithium is generally accepted to be the most mobile species. This has been demonstrated in numerous experimental studies on $LiNbO_3$ with different Li/Nb ratios and oxygen partial pressures, using impedance spectroscopy and, mainly, NMR techniques [16–18,20–22]. With regard to oxygen tracer diffusion there is only one set of data in the literature. Diffusion coefficients were obtained by analysing the depletion rate of ^{18}O from the gas phase during $^{18}O/^{16}O$ isotope exchanges of presumably Li_2O-rich single crystals [23]. Because of the inherent problems associated with gas phase analysis of isotope exchange between a gas and a solid and the consequent doubts about the fairly low activation enthalpy reported ($\Delta H = 123$ kJ/mol), and because the exact composition of the Li_2O-rich single crystals used was not reported, there is a clear need to study oxygen diffusion in carefully characterised $LiNbO_3$ single crystals.

In the present work, SIMS is utilized in combination with $^{18}O/^{16}O$ gas phase exchange to investigate the oxygen diffusion and surface exchange in a Li_2O-deficient $LiNbO_3$ in the temperature interval 983–1188 K. This technique is an extremely reliable experimental method for studying oxygen diffusion in oxides [24].

2. Experimental

The $LiNbO_3$ single crystal was supplied by MaTecK (Jülich, Germany). Rietveld refinement of the Guinier pattern showed that the cell parameters are $a = 5.15289$ Å, $c = 13.87161$ Å. The calculated cell volume (318.977 Å^3) corresponds to a Li_2O content of about 47.1 mol% [25,26]. The intrinsic UV absorption was corrected for the reflected light and compared with the data in Ref. [27]. The absorption edge position (taken at absorption coefficient = 20 cm^{-1}) corresponds to a composition of about 46.4 mol% Li_2O [28]. The chemical analysis by ICP-AES showed that the crystal contained the following impurities (in ppm): Mg (1), Al (115), Ca (292), Cr (7), Mn (61), Fe (71), K (229), Na (269). The samples ($\approx 4 \times 4 \times 1$ mm^3) were cut in such a way that the optical c-axis was perpendicular or parallel to the large surfaces. One of the large surfaces was polished with diamond paste down to 1 μm and cleaned with ethanol in an ultrasonic bath. To remove stress induced by the polishing, all samples were pre-annealed in pure $^{16}O_2$ gas (200 mbar) at 1223 K for about 15 h. For the actual diffusion run the samples were placed on an alumina holder and were then introduced into the cold zone of the furnace, which was subsequently evacuated to a pressure of about 10^{-3} mbar. No reaction was observed between the samples and the alumina support. After evacuation, $^{16}O_2$ gas was introduced into the furnace at a pressure of 200 mbar. (This pressure was chosen as it corresponds to the oxygen activity in air and as it is not too different from the pressure used in the only existing reference study by Jorgensen and Bartlett (93 mbar) [23] – especially if the generally weak power-law dependence of defect concentrations on oxygen partial pressure is taken into account. Determination of the oxygen partial pressure dependence of the oxygen tracer diffusion coefficient was beyond the scope of the present study.) Prior to the ^{18}O exchange experiments all samples were once more pre-annealed in $^{16}O_2$ gas for a duration appreciably longer than the diffusion experiment to achieve thermodynamical equilibrium at the given temperature (see Table 1).

At the end of the $^{16}O_2$ pre-annealing step the furnace was evacuated down to 10^{-3} mbar and subsequently filled with ^{18}O-enriched gas. The exact ^{18}O gas concentration in the furnace, c_g, was measured by a residual gas analyser (RGA 200, Stanford Research Systems) to be 95% ^{18}O. A mechanical feed-through manipulator allowed to rapidly introduce the sample holder into the hot zone of the furnace, or to withdraw it, respectively. For typical average heating (and cooling) rates, α, of about 10 K/s, the total time correction of the diffusion time, $\Delta t \approx 2RT_{\mathrm{diff}}^2/\alpha\Delta H_a$, is less than 10 s for the diffusion temperatures, T_{diff}, and activation enthalpies, ΔH_a, of our experiment.

The diffusion profiles of the ^{18}O tracer were determined by time-of-flight secondary ion mass spectrometry (ToF-SIMS) on a TOF-SIMS IV instrument (IONTOF GmbH, Germany). A detailed description of the analysis method is given in Ref. [29]. The analytical conditions were as follows. Secondary ions for analysis were generated with 25 keV Ga^+ ions (burst mode) raster scanned over (60 μm)^2 with the cycle time set at 50 μs ($I_{dc} = 1.7$ nA). Sputter etching of the surface was accomplished with 2 keV Cs^+ ions raster scanned over (250 μm)^2 ($I = 130$ nA). Under these conditions the depth resolution is at most a few nanometers, according to Monte Carlo simulations [29]. Charging effects were prevented by coating the samples with gold (film thickness, 37 nm) and by flooding the sample surface with ~20 eV electrons ($I > 1$ μA). Negative secondary ions were monitored. Crater depths were measured with an accuracy of about 3% post analysis by interference microscopy (NT1100, Veeco Instruments Inc., NY, USA). A typical ToF-SIMS depth profile of an exchanged single crystal sample of $LiNbO_3$ is shown in Fig. 1. Together

Table 1
Annealing conditions for single crystalline $LiNbO_3$ samples

Orientation	Pre-annealing in $^{16}O_2$ (200 mbar)				Annealing in $^{18}O_2$ (200 mbar)	
	Stress removal		Equilibration			
	T (K)	Time (h)	T (K)	Time (h)	T (K)	Time (s)
∥	1223	15	1188	6	1188	4200
∥	1223	15	1073	92	1073	23 700
∥	1223	14	983	276	983	184 200
⊥	1223	15	1188	6	1188	4200
⊥	1223	15	1073	92	1073	23 700
⊥	1223	14	983	276	983	184 200

∥: Diffusion is parallel to the optical c-axis; ⊥: diffusion is perpendicular to the optical c-axis. (The error in the temperature measurement was approximately ±3 K.)

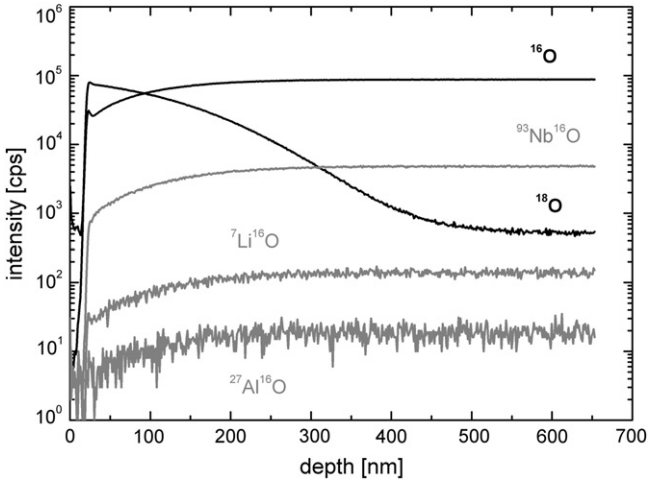

Fig. 1. Typical raw data of ToF-SIMS depth profiles of an oxygen exchanged single crystal sample of $LiNbO_3$ (1073 K, 23 700 s, diffusion is parallel to the optical c-axis). The initial portion of the profile corresponds to the gold film (37 nm) used to aid charge compensation.

with the complementary signals for ^{18}O and ^{16}O, the $M^{16}O$ signals ($M = {}^{7}Li$, ^{93}Nb and ^{27}Al) for the two matrix elements and a typical trace impurity (Al), respectively, are given in Fig. 1, all showing the same complementary behaviour.

At thermodynamic equilibrium the ^{16}O isotope flux out of the sample equals the ^{18}O isotope flux into the sample (neglecting the very low concentration of ^{17}O), which yields

$$c_{^{16}O}(x,t) + c_{^{18}O}(x,t) = c_O^{tot} = \text{constant} \tag{1}$$

where $c_{^{16}O}$, $c_{^{18}O}$ and c_O^{tot} are the concentrations of ^{16}O, ^{18}O and total oxygen.

The instrumental mass fractionation that occurs during the measurement of oxygen isotope ratios by ToF-SIMS is negligible compared to the error arising from counting statistics. In addition, the two oxygen isotopes are chemically identical. One may thus convert the intensity signals, I, of the measured oxygen isotopes into the ^{18}O atomic fraction, c, as follows

$$c = \frac{I(^{18}O)}{I(^{18}O) + I(^{16}O)} \tag{2}$$

For the sake of simplicity, the term ''relative concentration'' is used instead of atomic fraction throughout the text following below.

For oxygen incorporation at the crystal surface the standard phenomenological description of a first order reaction is adopted

$$j_{18}^{in} = \left(c_g - c_s\right)\, k \tag{3}$$

where j_{18}^{in} is the flux of ^{18}O from the gas phase at the solid surface, k is the surface exchange coefficient of oxygen, c_g is the ^{18}O concentration in the gas phase, and c_s is the ^{18}O concentration in the solid at the specimen surface. This flux must be equal to the diffusional flux of ^{18}O into the bulk of the sample, i.e. at $x = 0$

$$-D\left(\frac{\partial c}{\partial x}\right)_{x=0} = \left(c_g - c_s\right)k \tag{4}$$

where D is the oxygen tracer diffusion coefficient. The solution of the diffusion equation for such a boundary condition is given by Crank [30].

$$c(x,t) - c_\infty = \left(c_g - c_\infty\right)\left[\operatorname{erfc}\left(\frac{x}{\sigma}\right) - \exp\left(2\,\frac{x}{\sigma}\sqrt{\frac{t}{\tau}} + \frac{t}{\tau}\right) \times \operatorname{erfc}\left(\frac{x}{\sigma} + \sqrt{\frac{t}{\tau}}\right)\right] \quad \text{with} \quad \sigma = 2\sqrt{Dt} \text{ and } \tau = \frac{D}{k^2} \tag{5}$$

where c_g is the constant ^{18}O gas concentration in the gas phase, c_∞ the natural abundance of ^{18}O in the sample (for $x = \infty$), σ the diffusion length, and τ a characteristic time constant. The physical meaning of τ is obvious if one considers the time dependence of the ^{18}O concentration near the surface of the solid, $c_s(t) = c(x = 0,t)$

$$c_s(t) - c_\infty = \left(c_g - c_\infty\right)\left[1 - \exp\left(\frac{t}{\tau}\right)\operatorname{erfc}\left(\sqrt{\frac{t}{\tau}}\right)\right] \tag{6}$$

The characteristic time constant, τ, determines the duration that is necessary to reach equilibrium between the ^{18}O concentration in the gas phase and the ^{18}O concentration at the surface of the solid.

Fig. 2 shows typical SIMS depth profiles of the relative ^{18}O concentration measured in single crystal $LiNbO_3$ after diffusion annealing in an $^{18}O_2$ gas atmosphere (200 mbar). Samples of both orientations were placed together in the furnace for the same duration (at $T = 983$ K, $t = 184\,200$ s), in order to achieve identical diffusion treatments. It is seen

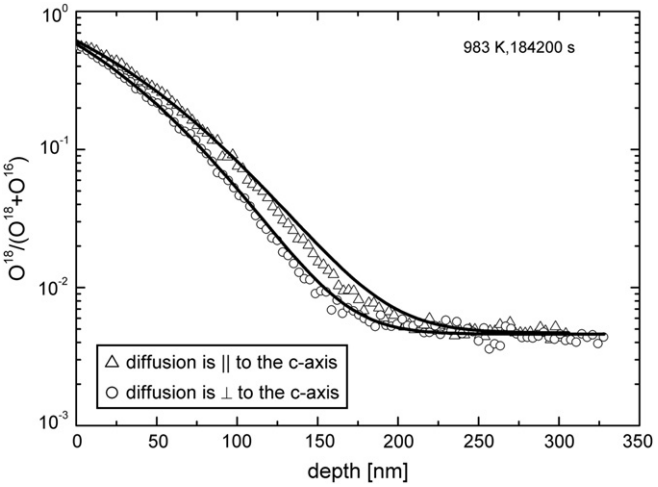

Fig. 2. Typical ToF-SIMS depth profiles of the relative ^{18}O concentration measured in single crystal $LiNbO_3$ after a diffusion experiment at 983 K for 184 200 s in an $^{18}O_2$ gas atmosphere (200 mbar). The solid lines represent mean squares fits using Eq. (5).

(Fig. 2) that the penetration depth along the optical c-axis is slightly larger than perpendicular to it. At present it is difficult to judge whether this difference is significant or not. On the one hand, the penetration depths at all investigated temperatures are larger for diffusion parallel to the c-axis in comparison to diffusion perpendicular to it; on the other hand, the differences between the resulting diffusivity values lie within the error limits of the measurements (see below). Measurements at lower temperatures would prove useful, in view of the fact that the ratio of the experimentally determined diffusivities, $D_{\parallel}/D_{\perp}$, appears to increase slightly with decreasing temperature (see Table 2). The solid lines in Fig. 2 are the result of a mean squares fit procedure to Eq. (5).

The measured background value of ^{18}O is about 0.004, whereas its natural abundance is 0.002. This deviation, whose origin is uncertain, is, however, of no importance for the evaluation of the diffusion profiles and the diffusivity data obtained from the evaluation. (One possible reason for a deviation is reported by De Souza and Chater [31]. They found that the ^{18}O fraction in pre-annealing gases might be significantly higher than the literature value of 0.204% [32]. By means of simulations they showed that the effects are important when analyzing grain boundary diffusion, but can be neglected when investigating bulk diffusion and surface exchange, as is the case here.)

The actual fit parameters determined from the measured SIMS depth profiles are the diffusion length, σ, and the reduced annealing time, t/τ (see Eq. (5)). From these fit parameters one can calculate the physical parameters D and k, because the annealing time, t, is measured independently. For $t/\tau > 10$ the calculated surface exchange coefficient, k, will be erroneous because of error accumulation, which induces errors of several hundred percent [33]. This t/τ regime has therefore to be avoided.

To evaluate the surface exchange coefficient, k, it is necessary to measure quantitatively the ^{18}O concentration in the gas phase, c_g, and in the solid surface, c_s. Only if these concentrations are measured by different methods (here: residual gas analysis for c_g and SIMS for c_s) they contribute independently to the error accumulation. Simple error estimation is possible in the following way: Eq. (6) can be approximated with errors less than 10% for $t/\tau \geq 3$ by the following equation [33]

$$c_s(t) - c_\infty \cong (c_g - c_\infty)\left(1 - \frac{1}{\sqrt{\pi}}\sqrt{\frac{\tau}{t}}\right) \text{ for } \frac{t}{\tau} \geq 3 \tag{7}$$

Neglecting the small background value, c_∞, and taking into account $\tau = D/k^2$ we obtain the following approximate equation for the surface exchange coefficient

$$k \cong \frac{1}{\sqrt{\pi}}\sqrt{\frac{D}{t}}\frac{c_g}{c_g - c_s} \text{ for } \frac{t}{\tau} \geq 3 \tag{8}$$

As time measurement errors in the order of 10 s (see respective comment in Section 2) are practically negligible, with annealing times of several thousand seconds (see Table 2) the relative error of k is approximately given by

$$\left|\frac{\Delta k}{k}\right| \cong \left|\frac{\Delta x}{x}\right| + \frac{c_s}{c_g - c_s}\left(\left|\frac{\Delta c_g}{c_g}\right| + \left|\frac{\Delta c_s}{c_s}\right|\right) \text{ for } \frac{t}{\tau} \geq 3 \tag{9}$$

where $\Delta x/x$ is the percentage error of the SIMS crater depth measurement. If one assumes an error of both the concentration measurements, $\Delta c_g/c_g$ and $\Delta c_s/c_s$, and the SIMS crater depth measurement of about 4%, one calculates an error for the k values measured at 1073 K of about 50% ($t/\tau \approx 14$, see Table 2), which is presumably masked by the (probably even larger) errors in k due to variations in the surface finish. However, even for the same surface state the relative error in k must be larger than the relative error in D, which is mainly $|\Delta D/D| \cong 2|\Delta x/x|$ [33].

A compilation of the mean squares fit results and all the experimental parameters is given in Table 2. The straight lines in Fig. 3 have been drawn based on the following Arrhenius relations for D and k

$$D = \left(6.4^{+6.3}_{-3.2}\right) \times 10^{-3}\ \mathrm{m^2/s} \exp\left(-\frac{(333 \pm 6)\mathrm{kJ/mol}}{RT}\right) \quad \text{for } 983\ \mathrm{K} \leq T \leq 1188\ \mathrm{K} \tag{10}$$

$$k = \left(7.8^{+168}_{-7.4}\right) \times 10^{2}\ \mathrm{m/s} \exp\left(-\frac{(288 \pm 27)\mathrm{kJ/mol}}{RT}\right) \quad \text{for } 983\ \mathrm{K} \leq T \leq 1188\ \mathrm{K} \tag{11}$$

with $R = 8.314\ \mathrm{J\ mol^{-1}\ K^{-1}}$.

3. Results and discussion

The diffusivity is a second-rank tensor, which for a hexagonal system will be isotropic in the basal plane and different for the direction perpendicular to it. For the range of temperatures examined here, however, no significant differences were found between oxygen diffusion or surface exchange coefficients measured perpendicular and parallel to the optical c-axis.

Table 2
Compilation of all experimental parameters (see text for an estimation of the most significant errors)

Orientation	T (K)	t (s)	c_g	c_∞	t/τ	σ (nm)	c_s	τ (s)	D (m^2/s)	k (m/s)
∥	983	184 200	0.95	0.0047	1.73	103.4	0.61	106 474	1.45×10^{-20}	3.69×10^{-13}
∥	1073	23 700	0.95	0.0035	13.7	210.2	0.81	1730	4.66×10^{-19}	1.64×10^{-11}
∥	1188	4 200	0.95	0.003	8.4	493.6	0.76	500	1.45×10^{-17}	1.70×10^{-10}
⊥	983	184 200	0.95	0.0046	1.3	90.5	0.58	141 692	1.11×10^{-20}	2.80×10^{-13}
⊥	1073	23 700	0.95	0.0039	14.2	200.4	0.81	1669	4.24×10^{-19}	1.59×10^{-11}
⊥	1188	4200	0.95	0.0036	4.0	486.5	0.71	1050	1.41×10^{-17}	1.16×10^{-10}

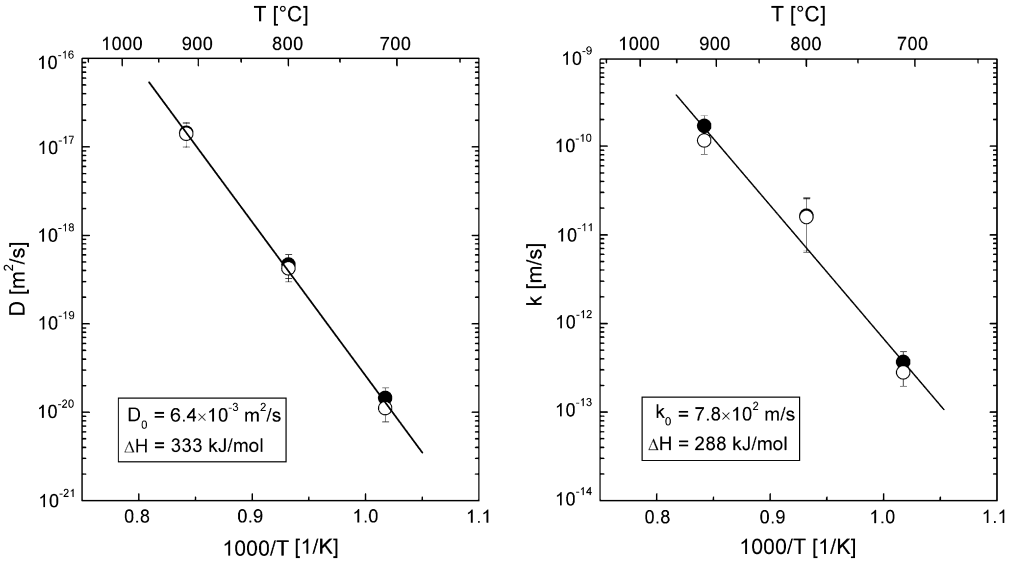

Fig. 3. Oxygen diffusion coefficients (left) and oxygen surface exchange coefficients (right) measured in single crystal $LiNbO_3$. Solid points: diffusion is parallel to the optical *c*-axis. Open points: diffusion is perpendicular to the optical *c*-axis.

This agrees with electrical conductivity measurements [34,35] and chemical diffusion measurements (of "Li_2O" into $LiNbO_3$) [34], for which only minor differences along the different crystallographic orientations were observed. This may be due to the constant lattice spacing along the *c*-axis (which increases only very little between room temperature and a shallow maximum at about 970 K, before it decreases to a value slightly smaller than the room temperature value at about 1270 K) and the expansion of the lattice spacing along the *a*-axis (which increases almost linearly from its room temperature value to a value of about 0.521 nm at about 1170 K, before it increases strongly to a value of about 0.529 nm at about 1470 K) as the temperature is increased within the measured temperature range (973–1073 K) [36]. Birnie III [15], in his review of diffusion data in $LiNbO_3$, pointed out that diffusion is fairly close to isotropic for H, Li, O, Ti, Mg, and Er also. Taking into account usual errors in diffusion measurements and the apparent discrepancies between the different studies quoted in Ref. [15] the author himself does not dwell on the orientation dependency. In their work on oxygen diffusion in Li_2O-rich $LiNbO_3$, Jorgensen and Bartlett [23] did not detect any anisotropy either. Furthermore, proton exchange in quasi-stoichiometric $LiNbO_3$ did not show any anisotropy [37]. Similarly, no significant anisotropy was observed for the oxygen diffusivity in single crystalline 2/1-mullite [38]. This clearly shows that simple arguments based on crystallographic features (mullite is a silicate with a pronounced anisotropy of the "oxygen chains") can be strongly misleading.

The small diffusion coefficient obtained for oxygen implies that oxygen ions cannot be regarded to be mainly responsible for the electrical conductivity in $LiNbO_3$ single crystals. In the previous work by Jorgensen and Bartlett [23], the high-temperature transport in $LiNbO_3$ was investigated by electrical conductivity measurements which showed that at $p_{O_2} = 0.981$ bar the conductivity was ionic, whereas it was electronic and proportional to $p_{O_2}^{-1/4}$ at $p_{O_2} < 10^{-6}$ bar. This behaviour was attributed to singly ionised oxygen vacancies, $V_O^{\bullet}$, with a formation enthalpy of 409 kJ/mol [23]. In the same publication the only oxygen tracer diffusion data for $LiNbO_3$ available in the literature is reported. The oxygen diffusivity was obtained from the rate of $^{18}O_2$ depletion from a limited volume of $^{16}O_2/^{18}O_2$ gas at a partial pressure of 93 mbar. Only the residual $^{18}O_2$ concentration in the gaseous phase was measured with this method. This may lead to inaccuracies, mainly because ^{18}O was diluted with ^{16}O to yield an $^{18}O/^{16}O$ ratio of 5–10%. The individual diffusion runs where stopped when the final fractional ^{18}O uptake reached more than 50%. The quoted authors could not exclude the possibility of leakage in the gas container and the absorption of $^{18}O_2$ on the surface of the experimental setup. Nevertheless, using the solution of Fick's second law for a plane sheet geometry and assuming fast surface exchange kinetics, the following Arrhenius expression for the tracer diffusivity of ^{18}O in the solid was derived [23].

$$D = \left(3.03^{+68}_{-2.9}\right) \times 10^{-10}\ \mathrm{m^2/s} \exp\left(-\frac{(123 \pm 29)\mathrm{kJ/mol}}{RT}\right) \quad \text{for } 973\ \mathrm{K} \le T \le 1273\ \mathrm{K} \tag{12}$$

This result is significantly different from the value obtained in the present work. The diffusion coefficients obtained are larger by 2.5–4 orders of magnitude than ours over the measured temperature range. The activation energy of 123 kJ/mol is much lower than our value of 333 kJ/mol.

The electrical transport measurement together with the oxygen diffusion data showed that the electrical conductivity of $LiNbO_3$ at 0.981 bar of oxygen is not determined by oxygen [23] as the obtained transport number of oxygen is much less than unity. Taking into account that Nb^{5+}, although smaller than Li^+, has a relatively large charge, and thus is not likely to be very mobile, it is obvious that Li^+ is the most mobile

ionic species. On the other hand, to enable oxygen transport oxygen interstitials or oxygen vacancies must exist in the crystal even if the concentrations of these minority defects (which virtually do not appear in the electroneutrality condition as given below) may be very low. (Contrary to older models for OH incorporation on oxygen vacancies recent studies discard this mechanism for a fairly wide range of Li_2O deficiency [28,37].)

An observed increase in the density of the Nb_2O_5-rich composition could not be interpreted by an oxygen vacancy model, implying that oxygen vacancies are not responsible for the non-stoichiometry in $LiNbO_3$ [1,8,25,39,40]. Smyth [41] proposed a model to account for both the Li_2O deficiency and the increase in density observed as a result of reduction. He discounted the possibility of oxygen vacancies being the predominant defects in Nb_2O_5-rich $LiNbO_3$ and assumed a high degree of ionic disorder in cation stacking similar to the ilmenite structure [35,41]. The results of computer-simulation studies [41,42] are compatible with Smyth's model. Although it is thus still not clear if Li_2O deficiency is accommodated via V'_{Li} or by $Nb^{4\bullet}_{Li}$ and $V^{5\prime}_{Nb}$ (or both mechanisms simultaneously) [37], this controversy is not important for our discussion of oxygen transport via intrinsic minority defects or extrinsic defects.

Based on the description given above we present the following discussion of the high activation energy of diffusion, $\Delta H_D = 333$ kJ/mol, that we obtained. The two key points are that the single crystals we used were Li_2O-deficient, and that oxygen diffusion takes place by a vacancy mechanism. If a (conservative) analytical error of ± 0.1 mol% Li_2O is accepted it can be assumed that at the three experimental temperatures our sample material, if correctly equilibrated (see Table 1), was in equilibrium with the neighbouring $LiNb_3O_8$ phase, and thus Li_2O-deficient with respect to the congruently melting composition (≈ 48.5 mol% Li_2O). Depending on the quenching rate after annealing we observed in some cases a reduced transparency of the crystals, which indicates that precipitates formed which most probably consisted of $LiNb_3O_8$ [44]. Below we first discuss the situation in pure $LiNbO_3$, i.e. intrinsic defects only (case A). Afterwards, the effect of aliovalent vacancies, i.e. extrinsic defects, is discussed (case B).

3.1. Case A: intrinsic defects

According to Refs. [41,42] the most probable electroneutrality condition for Li_2O-deficient samples is $4[Nb^{4\bullet}_{Li}] = [V'_{Li}]$. It corresponds to the majority intrinsic defects involved in the reaction

$$9LiNb_3O_8 + 15Li^x_{Li} \Leftrightarrow 3Nb^{4\bullet}_{Li} + 12V'_{Li} + 24LiNbO_3 \tag{13}$$

The (very low) oxygen vacancy concentration is consequently governed by the Li_2O Schottky equilibrium. The Li_2O Schottky equilibrium in a Li_2O-poor crystal, which is in equilibrium with the neighbouring phase $LiNb_3O_8$, reads

$$2Li^x_{Li} + O^x_O + LiNb_3O_8 \Leftrightarrow 2V'_{Li} + V^{\bullet\bullet}_O + 3LiNbO_3 \tag{14}$$

As there are no thermodynamic data available for this reaction, we consider the virtual reaction

$$2Li^x_{Li} + O^x_O \Leftrightarrow Li_2O + 2V'_{Li} + V^{\bullet\bullet}_O \tag{15}$$

for which Donnerberg et al. [42] calculated 1.94 eV per defect. Araujo et al. [43] recently calculated 1.80 eV per defect. Inserting the electroneutrality condition into the mass action law equation for Eq. (15) one finally gets

$$\Delta H^{Li_2O}_{Schottky} = -2R\frac{d\ln[Nb^{4\bullet}_{Li}]}{d(1/T)} - R\frac{d\ln[V^{\bullet\bullet}_O]}{d(1/T)} = \Delta H^{Nb_2O_5}_{Sol} + \Delta H_{V^{\bullet\bullet}_O} \tag{16}$$

The first term on the right hand side of Eq. (16), $\Delta H^{Nb_2O_5}_{Sol}$, can be estimated from the solubility limit on the Li_2O-deficient side of the phase diagram [8,44]: it is less than about 10 kJ/mol and can therefore be neglected, taking into account the experimental error bars given in Ref. [44] and the discrepancy between the two calculated values in Refs. [42,43].

In the intrinsic case the measured activation enthalpy of diffusion then consists of the sum of the migration enthalpy of oxygen vacancies, ΔH_{migr}, and the enthalpy of Li_2O Schottky disorder, $\Delta H^{Li_2O}_{Schottky}$. Using atomistic simulation methods Donnerberg et al. [42] obtained a value of 562 kJ/mol for $\Delta H^{Li_2O}_{Schottky}$, Araujo et al. [43] found 521 kJ/mol. If these values were realistic, both our own experimentally determined value of the activation enthalpy, 333 kJ/mol, as well as Jorgensen and Bartlett's value, 123 kJ/mol, would be by far too small. We therefore conclude that the calculated values for the Li_2O Schottky defect are too high.

An alternative interpretation, however, would allow us to reconcile the differences between our results and those of Jorgensen and Bartlett [23]. They performed oxygen tracer diffusion experiments on samples that were equilibrated with Li_2O powder, but did not mention any formation of a (neighbouring) second phase which should have been Li_3NbO_4. Their samples were, however, presumably Li_2O-rich. The most probable electroneutrality condition in this case comprises Li^+ ions on Nb^{5+} sites, $Li^{\prime\prime\prime\prime}_{Nb}$, being compensated by oxygen vacancies, $V^{\bullet\bullet}_O$, according to the reaction

$$Nb^x_{Nb} + 2O^x_O + Li_3NbO_4 \Leftrightarrow Li^{\prime\prime\prime\prime}_{Nb} + 2V^{\bullet\bullet}_O + 2LiNbO_3 \tag{17}$$

According to the well investigated phase diagram of the system Li_2O–Nb_2O_5 the solubility of Li_3NbO_4 in $LiNbO_3$ is virtually independent of temperature. Therefore the induced oxygen vacancy concentration is also independent of temperature, which means that the activation energy determined by Jorgensen and Bartlett [23], $\Delta H = 123$ kJ/mol, corresponds practically solely to the migration enthalpy, ΔH_{migr}. Thus, if we take their data to be accurate, we find that the formation enthalpy of the Li_2O Schottky defect, $\Delta H^{Li_2O}_{Schottky}$, should amount to $333 - 123$ kJ/mol $= 210$ kJ/mol (confer Eqs. (10) and (12) as well us our comment on $\Delta H^{Nb_2O_5}_{Sol}$ in Eq. (16) estimated from Ref. [44]).

3.2. Case B: extrinsic defects

Aliovalent cations can be incorporated in numerous ways into the $LiNbO_3$ lattice. Unfortunately, in Ref. [43] only substitution reactions for divalent and trivalent cations were considered which do not yield oxygen vacancies as induced defects. However, such reactions cannot be excluded, like, e.g.

$$LiNbO_3 + 2MO + 2Nb^{x}_{Nb} + 3O^{x}_{O} \Leftrightarrow 2M'''_{Nb} + 3V^{\bullet\bullet}_{O} + LiNb_3O_8 \quad (18)$$

for divalent cations, and

$$LiNbO_3 + M_2O_3 + 2Nb^{x}_{Nb} + 2O^{x}_{O} \Leftrightarrow 2M''_{Nb} + 2V^{\bullet\bullet}_{O} + LiNb_3O_8 \quad (19)$$

for trivalent cations. Taking only impurities with compatible ionic radius from the list given in Section 2 (e.g. Al^{3+}: 67.5 pm vs. Nb^{5+}: 78 pm in six-fold oxygen coordination [45]) and assuming that the solubility limits are higher than 100–200 ppm, the induced oxygen vacancy concentrations are independent of temperature and much higher than the intrinsic oxygen vacancy concentration. Our experimentally determined oxygen activation enthalpy thus would correspond to the enthalpy of migration, ΔH_{migr}, only. As we have no information on the kind and the level of possible impurities of the crystals used by Jorgensen and Bartlett [23] their fairly small value of the activation enthalpy remains unexplained in the picture of extrinsic defects.

Comparing the experimental values of the pre-exponential factors, D_0 (see Eqs. (10) and (12)), the picture is not simple either: an estimated value of the activation entropy of $\Delta S/k_B \approx 7\ldots8$ (cf. Eq. (10)) in our present work can be qualitatively rationalized as it comprises the (definitely positive) formation entropy of the Li_2O Schottky defect together with a (probably) smaller contribution from the migration entropy, ΔS_{migr}. If one estimates this latter term using the standard harmonic approximation, i.e. $\Delta S_{migr}/k_B = -\sum \ln(\nu_{i,s}/\nu_{i,0})$, where $\nu_{i,s}$ and $\nu_{i,0}$ are the normal-mode frequencies for vacancy–ion pairs at the saddle point and in the equilibrium position, respectively, one in general obtains, at best, a relatively small negative value, which would hardly explain a value of $\Delta S/k_B \approx -9$ as calculated from Eq. (12), taken from Ref. [23].

At present a comprehensive discussion of the surface exchange of oxygen as a function of the Li/Nb ratio is not yet possible; we restrict ourselves therefore to the remark that, for Li_2O-deficient $LiNbO_3$, the transport data fall on the electron-rich branch of the *h*-plane plot ($\ln k$ vs. $\ln D$) and exhibit a slope of $\partial \ln k(T)/\partial \ln D(T) = \Delta H_k/\Delta H_D = 0.86 \pm 0.10$ (for comparison with the corresponding data for other mixed conductors, see Refs. [46–48]).

4. Conclusions

We employed gas phase isotope exchange in combination with SIMS depth profiling to obtain precise data for oxygen tracer diffusion and surface exchange in Li_2O-deficient $LiNbO_3$. We propose that oxygen diffuses via extrinsic oxygen vacancies whose concentration is fixed by divalent and/or trivalent impurity cations incorporated on Nb^{5+} sites and that therefore the measured activation enthalpy of diffusion essentially consists of one term: the migration enthalpy of oxygen vacancies, ΔH_{migr}. For the intrinsic case, $\Delta H^{Li_2O}_{Schottky}$ can be estimated to be about 210 ± 45 kJ/mol and thus would not agree with two sets of calculated values, which amount to 540 ± 20 kJ/mol.

Despite extensive literature data on defects and diffusion in $LiNbO_3$, many aspects of self-diffusion in this material are still unclear. In particular, precise data of oxygen diffusion in $LiNbO_3$ as a function of the Li/Nb ratio is required. Interpretation of such data would be aided by extensive computer simulations of the relevant defect processes.

Acknowledgements

Financial support from Deutsche Forschungsgemeinschaft (DFG) is gratefully acknowledged. Thanks to the following persons from the Institut für Mineralogie, Leibniz Universität Hannover: Dr. C. Rüscher for the UV–vis measurements, Dr. S. Freimann for measuring the Guinier XRD pattern of the single crystalline $LiNbO_3$, and to Dr. T. Gesing for Rietveld refinement of the XRD pattern. We also acknowledge the help of Prof. Dr. C. Vogt and her coworkers (Institut für Anorganische Chemie, Leibniz Universität Hannover) for the trace chemical analysis (ICP-AES) of the $LiNbO_3$ crystal.

References

[1] S.C. Abrahams, J.L. Bernstin, W.C. Hamiltons, H.J. Levinstein, J.M. Reddy, J. Phys. Chem. Solids 27 (6–7) (1966) 997.
[2] H.D. Megaw, Acta Crystallogr., Sect. A 24 (6) (1968) 583.
[3] R.S. Weis, T.K. Gaylord, Appl. Phys. A 37 (1985) 191.
[4] A.M. Glass, Opt. Eng. 17 (5) (1978) 470.
[5] A.M. Glass, D. von der Linde, T.J. Negran, Appl. Phys. Lett. 25 (4) (1974) 233.
[6] M.M. Abouelleil, F.J. Leonberger, J. Am. Ceram. Soc. 72 (8) (1989) 1311.
[7] C.S. Tsai, Jpn. J. Appl. Phys. 19 (Suppl. 1) (1980) 661.
[8] P. Lerner, C. Legras, J. Dumas, J. Cryst. Growth 3 (4) (1968) 231.
[9] O.F. Schirmer, O. Thiemann, M. Wohlecke, J. Phys. Chem. Solids 52 (1) (1991) 185.
[10] H. Fay, W.J. Alford, H.M. Dess, Appl. Phys. Lett. 12 (3) (1968) 89.
[11] K. Nassau, M.E. Lines, J. Appl. Physiol. 41 (2) (1970) 533.
[12] S.C. Abrahams, P. Marsh, Acta Crystallogr., Sect. B 42 (1) (1986) 61.
[13] A. Räuber, in: E. Kaldis (Ed.), Current Topics in Materials Science, vol. 1, North-Holland, Amsterdam, 1978, p. 481.
[14] K. Wong (Ed.), Properties of Lithium Niobate, INSPEC, UK, 2002.
[15] D. Birnie III, J. Mater. Sci. 28 (1993) 302.
[16] M. Masoud, P. Heitjans, Defect Diffus. Forum 237–240 (2005) 1016.
[17] P. Heitjans, M. Masoud, A. Feldhoff, M. Wilkening, Faraday Discuss. 134 (2007) 67.
[18] J. Hennel, J. Klinowski, Fundamentals of Nuclear Magnetism, Longman Scientific and Technical, Harlow, 1993.
[20] D. Bork, P. Heitjans, J. Phys. Chem. B 105 (2001) 9162.
[21] M. Wilkening, D. Bork, S. Indris, P. Heitjans, Phys. Chem. Chem. Phys. 4 (2002) 3246.
[22] M. Wilkening, P. Heitjans, Solid State Ionics 177 (2006) 3031.
[23] P.J. Jorgensen, R.W. Bartlett, J. Phys. Chem. Solids 30 (1968) 2639.

[24] M. Martin, Diffusion in oxides, in: P. Heitjans, J. Kärger (Eds.), Diffusion in Condensed Matter – Methods, Materials, Models, Springer, Berlin, 2005, p. 209.
[25] N. Iyi, K. Kitamura, F. Izumi, J. Solid State Chem. 101 (1992) 340.
[26] M. Wohlecke, G. Corradi, K. Betzler, Appl. Phys. B – Lasers and Optics 63 (4) (1996) 323.
[27] I. Földvari, K. Polgar, R. Voszka, R.N. Balasanyan, Cryst. Res. Technol. 19 (12) (1984) 1659.
[28] Y. Kong, W. Zhang, X. Chen, J. Xu, G. Zhang, J. Phys.: Condens. Matter 11 (1999) 2139.
[29] R.A. De Souza, J. Zehnpfenning, M. Martin, J. Maier, Solid State Ionics 176 (15–16) (2005) 1465.
[30] J. Crank, The Mathematics of Diffusion, second ed. Oxford University Press, Oxford, 1975.
[31] R.A. De Souza, R.J. Chater, Solid State Ionics 176 (23–24) (2005) 1915.
[32] K.J.R. Rosman, P.D.P. Taylor, Pure Appl. Chem. 70 (1) (1998) 217.
[33] P. Fielitz, G. Borchardt, Solid State Ionics 144 (2001) 71.
[34] S. Bredikhin, S. Scharner, M. Klingler, V. Kveder, B. Redikin, W. Weppner, J. Appl. Physiol. 88 (10) (2000) 5687.
[35] A. Mehta, E.K. Chang, D. Smyth, J. Mater. Res. 6 (4) (1991) 851.
[36] S. Abrahams, H. Levinstein, J. Reddy, J. Phys. Chem. Solids 27 (1966) 1019.
[37] V.A. Alcázar de, J. Rams, J.M. Cabrera, F. Agulló-López, J. Appl. Physiol. 82 (1997) 4752.
[38] P. Fielitz, G. Borchardt, M. Schmücker, H. Schneider, M. Wiedenbeck, D. Rhede, S. Weber, S. Scherrer, J. Am. Ceram. Soc. 84 (12) (2001) 2845.
[39] W. Bollmann, Cryst. Res. Technol. 18 (9) (1983) 11047.
[40] L. Kovács, K. Polgar, Cryst. Res. Technol. 21 (6) (1986) K101.
[41] D.M. Smyth, Ferroelectrics 50 (1983) 93.
[42] H. Donnerberg, S.M. Tomlinson, C.R.A. Catlow, O.F. Schirmer, Phys. Rev. B 40 (1989) 11909.
[43] R.M. Araujo, K. Lengyel, R.A. Jackson, L. Kovács, M.E.G. Valerio, J. Phys.: Condens. Matter 19 (2007) 046211.
[44] L.O. Svaasand, M. Eriksrud, G. Nakken, A.P. Grande, J. Cryst. Growth 22 (1974) 230.
[45] R.D. Shannon, Acta Crystallogr. Sect. A 32 (1976) 751.
[46] J.A. Kilner, R.A. De Souza, I.C. Fullarton, Solid State Ionics 86–88 (1996) 703.
[47] R.A. De Souza, J.A. Kilner, Solid State Ionics 126 (1–2) (1999) 153.
[48] R.A. De Souza, Phys. Chem. Chem. Phys. 8 (7) (2006) 890.